IET Microwaves, Antennas & Propagation

Research Article

IET Journals
The Institution of Engineering and Technology

Improved ant colony algorithm for adaptive frequency-tracking control in WPT system

ISSN 1751-8725
Received on 28th February 2017
Revised 20th July 2017
Accepted on 23rd July 2017
E-First on 8th December 2017
doi: 10.1049/iet-map.2017.0159
www.ietdl.org

Yang Li[1], Cheng Zhang[1] ✉, Qingxin Yang[1], Jianxiong Li[2], Yaxi Zhang[1], Xian Zhang[1], Ming Xue[1]

[1]Tianjin Key Laboratory of Advanced Technology of Electrical Engineering and Energy, Tianjin Polytechnic University, Tianjin 300387, People's Republic of China

[2]College of Electronics and Information Engineering, Tianjin Polytechnic University, Tianjin 300387, People's Republic of China

✉ *E-mail: yxzhang_yxzhang@163.com*

Abstract: When the distance between resonators is low enough for the coupling condition to be greater than the critical coupling, the single resonant peak at the load splits to form double peaks. This frequency-splitting phenomenon results in a reduction in the power transferred. In this study, an adaptive frequency-tracking control (AFTC) approach based on a closed-loop control scheme is implemented to overcome this problem. An improved ant colony algorithm (IACA) was proposed in AFTC to track the maximum power point in real time. Then, simulations were performed to test the real-time characteristics of IACA. Finally, a wireless power transfer system with AFTC is demonstrated experimentally to validate the IACA results and the tracking of the optimal frequency.

1 Introduction

In recent years, wireless power transfer (WPT) technique via coupled magnetic resonances has been widely researched, and scientists at the Massachusetts Institute of Technology have exhibited middle-distance WPT using magnetic resonant coupling [1]. The advantages of increased coverage, high power, good penetrability, and high efficiency make WPT useful in the automotive industry [2, 3]. However, research into WPT systems that use coupled magnetic resonances is still in the initial stages, and there have been few theoretical and experimental analyses. In addition, there remain many problems that need to be solved, e.g. the decrease in transferred power decreases as the distance decreases. The reason for this phenomenon is that the resonance frequency of WPT systems is divided. The maximum transfer power is obtained only when WPT systems are resonant, and it is therefore necessary that the operation frequency of power sources and resonance frequency of resonators be the same.

There are two approaches to satisfy the resonance requirements [4, 5]. One is to match the resonance frequency of resonators to the operation frequency of the power source, while the other approach is to match the operation frequency of a power source to the resonance frequency of resonators. In [6], an impedance-matching network is used to vary the resonance frequency of resonators at a certain distance to 13.56 MHz using the former approach. To improve the transfer power in cases that involve varying distances between resonators, the method that achieves adaptive matching by tuning the receiver circuit and matching network was introduced [7]. However, with this approach, there is some difficulty in realising the matching of the input and output impedances, and it also increases the power loss of the system. Therefore, the latter approach needs to be considered, and a frequency-tracking method is used to satisfy the criteria. In [8], the frequency tracking of the load current using phase-locked loop (PLL) was implemented. In [9], a resonant-frequency-tracking method is presented using a digital signal processor based software PLL. In [10], the frequency-tracking method based on an integrated PLL is presented. Note that the above studies are based on inductively coupled power transfer systems, and the frequency tracked by the PLL does not exceed 1 MHz; therefore, the frequency-tracking method based on PLL is not suitable for WPT systems using coupled magnetic resonances. In [11], the resonant-frequency-tracking method based on the conventional perturbation and observation algorithm is presented by analysing the relationship between the operation frequency and output power. In [12], a multi-objective genetic algorithm is proposed for a WPT. The proposed algorithm maximises the transfer power by optimising the switching frequency of the full-bridge series-resonant inverter and the synchronous full-bridge rectifier output voltage, subject to their respective design constraints. These studies have made much progress towards frequency tracking. However, real-time frequency tracking has not been considered, which is key for moving devices.

In this paper, an improved ant colony algorithm (IACA) that adaptively adjusts the path pheromones is proposed to implement adaptive frequency-tracking control (AFTC) in WPT systems. The IACA can track the maximum power point in real time. Moreover, AFTC is based on a closed-loop control scheme that provides feedback regarding the required frequency, thus improving the transfer power significantly.

The rest of this paper is organised as follows: Section 2 analyses a WPT system with AFTC. In Section 3, the IACA is proposed. In Section 4, the characteristics of the AFTC based on IACA are analysed using simulation results. The experimental setup is described, and the results presented to verify the validity of IACA. Finally, Section 5 presents the conclusion.

2 Adaptive frequency-tracking (AFT) WPT system

The proposed AFT WPT system is illustrated in Fig. 1. A monolithic integrated direct digital synthesiser (DDS) is used to produce a high-frequency sinusoidal signal that is amplified by a power amplifier. Then, the power signal is transferred to the receiver via resonators. The high-frequency alternating current is rectified through the full-wave bridge rectified filter, and the voltage is stabilised using stabilised voltage circuit. Finally, the power is supplied to the load. Meanwhile, the voltage and current signals are processed by the power-detection module, and the results are transferred to a digital signal processor (DSP) using a ZigBee transceiver module. The IACA embedded in the DSP is triggered by the results, and it then outputs an optimal frequency to the DDS. The DDS then generates a sinusoidal signal having an optimal frequency, which can maximise the transfer power.

The AFTC system needs to achieve real-time adjustment of the source frequency, so it requires that the frequency can be accurately controlled in various scenarios. However, existing frequency-tracking systems need to be improved to be able to work

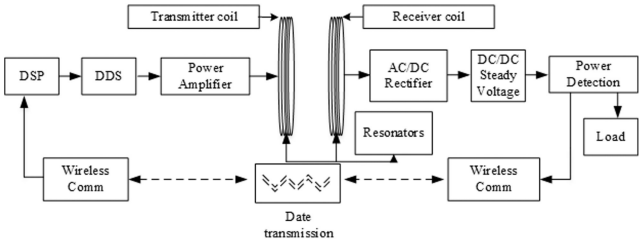

Fig. 1 *AFT WPT system*

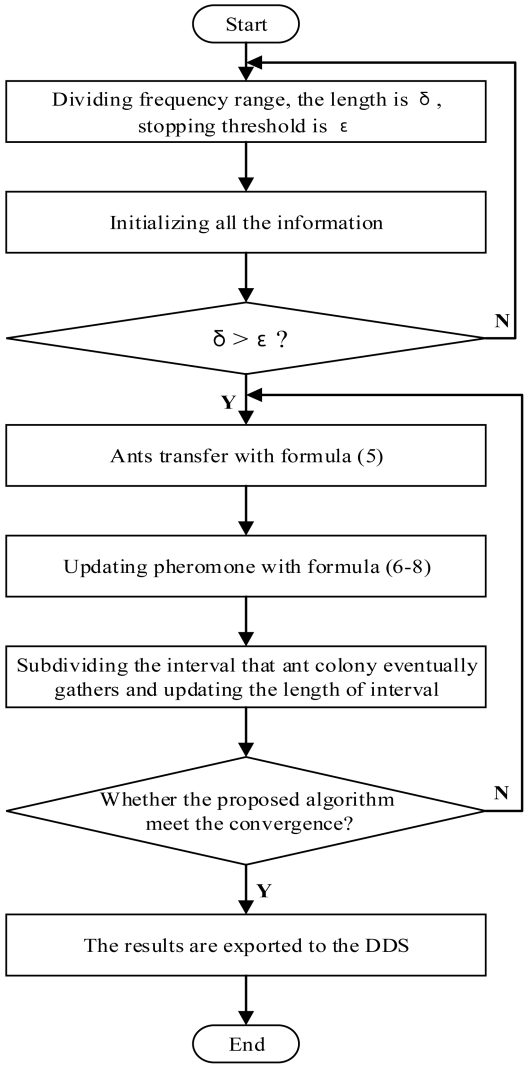

Fig. 2 *Flowchart of ant colony algorithm*

in real time, and thus an improved algorithm is proposed to adjust the source frequency in real time.

3 Improved ant colony algorithm

Compared with the ant colony algorithm, generic algorithms can effectively avoid local optimal solutions, but they have the defect of precocity [13]. Owing to better parallelism and self-organisation, the ant colony algorithm is a more mature and effective method that can reduce the time to initialise the population and calculate the maximum and minimum of the fitting function [14].

During the optimisation process, a single ant's behaviour is simple, but the behaviour of the entire ant colony can achieve a high level of cooperation using pheromones, and ants communicate via the pheromones indirectly; finally, they determine the optimal path through the collective behaviour of the ant colony. However, the traditional ant colony algorithm has a longer search time, and easily falls into local optimum owing to search stagnation. In other words, when the search has reached a certain point, all individuals will find the same solution, so they will not go further to determine the best solution in the solution space. Therefore, in this paper, an IACA that adaptively adjusts pheromones is proposed. The pheromones are adjusted by the intensity coefficient of pheromones, which varies with the number of iterations. Meanwhile, according to the states of the optimal and worst individual, the degree of positive feedback and negative feedback of pheromones is adjusted to avoid the prematurity of the algorithm in the early searching and latter converging stages. Thus, the proposed algorithm can be eliminated from the local optimum. In addition, to further avoid falling into the local optimum, the proposed algorithm expands the search space to meet the real-time requirements simultaneously.

The IACA process is shown in Fig. 2. The IACA is implemented by performing the following steps: (i) determine the initial distribution of the ant colony, (ii) determine the transition rules of the ant colony, (iii) update the pheromones, and (iv) reduce the search space of the ant colony. During the population initialisation, the effect of pheromones is not obvious, especially because of the discrepancy in the pheromone distribution at each point. However, the advantage of the point whose pheromone is better will appear only after a long time. To shorten the time, the following strategies are applied.

First, a heuristic function is considered to establish the initial search distribution of the ant colony in the initial stage of the algorithm. δ denotes the interval length and ε denotes the stop threshold. To increase the speed of the algorithm, the frequency interval is limited in 3.5–5.5 MHz according to the experimental results. When $\delta > \varepsilon$, the frequency interval is divided into N equal subintervals, where one subinterval is defined as follows:

$$I_i = [3.5 + (i-1)\delta, 3.5 + i\delta], \tag{1}$$

where x_i is the midpoint of I_i, which is as follows:

$$x_i = 3.5 + (i - 1/2)\delta \tag{2}$$

Each x_i value corresponds to a function $f(x_i)$. τ_i denotes the number of pheromones in subinterval I_i, and the initial value of the pheromone is estimated by $\tau_i(0) = \text{const}$, and the pheromone increment for each subinterval is set to zero ($\Delta\tau_i = 0$). Then, the neighbour (I_i) is on behalf of the interval set near I_i, shown as follows, for one-dimensional function:

$$\text{neighbour}(I_i) = \begin{cases} \{I_{i+1}\}, & i = 1 \\ \{I_{i-1}, I_{i+1}\}, & i = 2\ldots(n-1) \\ \{I_{i-1}\}, & i = n \end{cases} \tag{3}$$

Assuming that there is a virtual edge $e(I_i, I_j)$ between subinterval I_i and subinterval I_j, and that the weight of the edge is $|f(x_i) - f(x_j)|$, the heuristic function is represented as follows:

$$\eta_{ij} = |f(x_i) - f(x_j)| \tag{4}$$

If $f(x_i) - f(x_j) > 0$, ants in subinterval I_i will transfer to subinterval I_j; otherwise, they will not transfer. $P_{ij}^{(k)}$ denotes the probability that ant a_k can transfer to the next subinterval, which is calculated using the following equation:

$$P_{ij}^{(k)}(t) = \begin{cases} \dfrac{\tau_j^{\alpha}(t)\eta_{ij}^{\beta}}{\sum_{h \in \text{enable}_k} \tau_h^{\alpha}(t)\eta_{ih}^{\beta}}, & j \in \text{enable}_k \\ 0, & \text{otherwise} \end{cases} \tag{5}$$

Here, α is the relative influence of the pheromone trail, β denotes the relative influence of heuristic information, enable_k denotes the set of feasible nodes, and τ_j denotes the number of pheromones in subinterval I_j. If the ant a_k transfers from subinterval I_i to

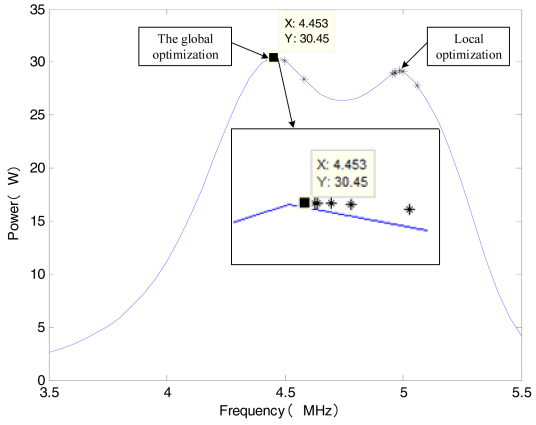

Fig. 3 *Simulation results*

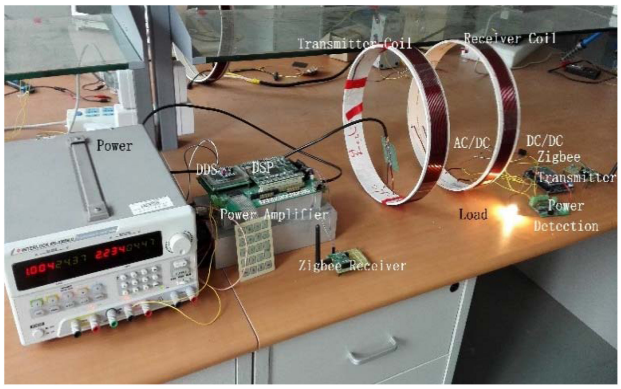

Fig. 4 *Frequency-tracking system*

subinterval I_j according to some probability, ant a_k will be in subinterval I_j and its deposited pheromone is designed as follows:

$$\Delta\tau_j^{\alpha}(t) = C_1\sigma'(\zeta)\left[f(x_i) - f(x_j)\right], \tag{6}$$

where C_1 is a constant that denotes the number of deposited pheromones; the larger the value of $f(x_i) - f(x_j)$, the greater the number of pheromones left by ants, so other ants are attracted to transfer to subinterval I_j. When the number of iterations is t, there are q ants transferring to subinterval I_j. These ants are $a_{j_1}, a_{j_2} \ldots a_{j_q}$, and the number of pheromones left by the ants is calculated as

$$\Delta\tau_i(t) = \sum_{p=1}^{q} \tau_j^{(jp)}(t) \tag{7}$$

When all of the transfers are finished, the total number of pheromones is determined by the evaporation rate of pheromones, which satisfies the following formula:

$$\tau_j(t+1) = (1-\rho)\tau_j(t) + \Delta\tau_j(t), \tag{8}$$

where ρ is the volatile coefficient of pheromones. To increase the search range and reduce the number of pheromones for the best and worst paths, the positive feedback of the algorithm is inhibited in the early search. Specifically, the value of ρ increases by 0.00015 more than for other individuals. In the latter search, the positive feedback of better individuals needs to be strengthened, so the strength coefficient C_1 of pheromones left by M individuals that have better fitness is σ times that of other individuals, and the value of ρ decreases by 0.0001 simultaneously. In addition, the value of M is one-sixth times that of the number of ants.

The search period is determined by the number of iterations as shown in the following equation:

$$\sigma'(\zeta) = \begin{cases} 0.6, & 0 \le \zeta \le 0.15 \\ -2.5\zeta + 1.2, & 0.15 < \zeta \le 0.3 \\ 2\zeta + 0.1, & 0.3 < \zeta \le 0.7 \\ 1.5, & 0.7 < \zeta \le 1 \end{cases} \tag{9}$$

Here, ζ denotes the evolutionary time and $\sigma'(\zeta)$ represents the pheromone changing coefficient. From (9), a large number of pheromones promote the population search. When $0.15 < \zeta \le 0.3$, the intensity coefficient of the pheromones gradually decreases. To avoid falling into a local optimum, the positive feedback should be suppressed. When $0.3 < \zeta \le 0.7$, the intensity coefficient of pheromones that belongs to optimal individuals should be increased so that it has a good advantage in terms of the number of pheromone elements. In the last stage of convergence, the intensity coefficient of the pheromones is maximum to ensure that the ants gather in the region of the optimal solution. Generally, pheromones distributed within the range where the function value is smaller, and thus, the ability of the interval to attract ants is greater.

When the iterations are stopped, the distribution of ants will exhibit the characteristics: all ants are distributed within the interval of the larger extreme point, and there are no ants in other intervals. Then, the interval is further subdivided to allow a search. When the interval is sufficiently small, the ants will be distributed near the larger extreme point. In addition, the middle position of the subinterval at which ants are distributed is the position of the extreme point.

4 Simulation and experiment results

During the IACA simulation, a large number of power points are sampled within the range of 3.5–5.5 MHz, corresponding to a fixed distance of 10 cm (critical coupling distance: 15 cm). Then, the frequency–power curve is fitted using the Gaussian function. The fitting formula is expressed as follows: (see (10)) Here f represents the load power and x represents the operation frequency. In the simulation, the number of ants in IACA is 19, the number of iterations is 10, $\alpha = 2$, $\beta = 3$, and $\rho = 0.6$. The pheromones of the interval are adaptively selected using (5)–(7). The simulation results are shown in Fig. 3.

The black point in Fig. 3 represents the maximum value of an individual ant and the local optimisation value. In addition, the power is 30.45 W at a distance of 10 cm between resonators at an operation frequency of 4.453 MHz (resonance frequency: 4.525 MHz).

Based on the simulation, the proposed frequency-tracking system based on IACA is implemented. A photograph of the system is shown in Fig. 4, and is composed of a power supply, DSP, DDS, power amplifier, resonators, rectifier circuit, power detection, and wireless communication modules. The coil parameters and frequencies of the transmitter and receiver are shown in Table 1, see the Appendix for the table of results.

To further illustrate the performance of the proposed algorithm, some experiments were carried out. The voltage waveforms of the transmitter and receiver are obtained when the distance between the transmitter and receiver is varied from 15 cm (critical coupling) to 10 cm (over coupling), as shown in Fig. 5*a* (without AFT) and Fig. 5*b* (with AFT). Then, the voltage waveforms of the transmitter and receiver are obtained when the distance between the transmitter and receiver is varied from 10 cm (over coupling) to 15 cm (critical coupling), as shown in Fig. 5*c* (without AFT) and Fig. 5*d* (with AFT).

The upper curve represents the voltage waveform of the transmitter (peak-to-peak: 72 V), and the lower curve represents the voltage waveform of the receiver (peak-to-peak: 23.2 V) in

$$\begin{aligned} f = {} & 8.753\mathrm{e}^{-(x-4.497)/0.8898^2} + 2.653\mathrm{e}^{-(x-4.993)/0.1007^2} - 403.5\mathrm{e}^{-(x-4.965)/0.2937^2} \\ & + 31.65\mathrm{e}^{-(x-4.618)/0.4505^2} + 129.7\mathrm{e}^{-(x-4.86)/0.248^2} + 310\mathrm{e}^{-(x-5.021)/0.2767^2} \end{aligned} \tag{10}$$

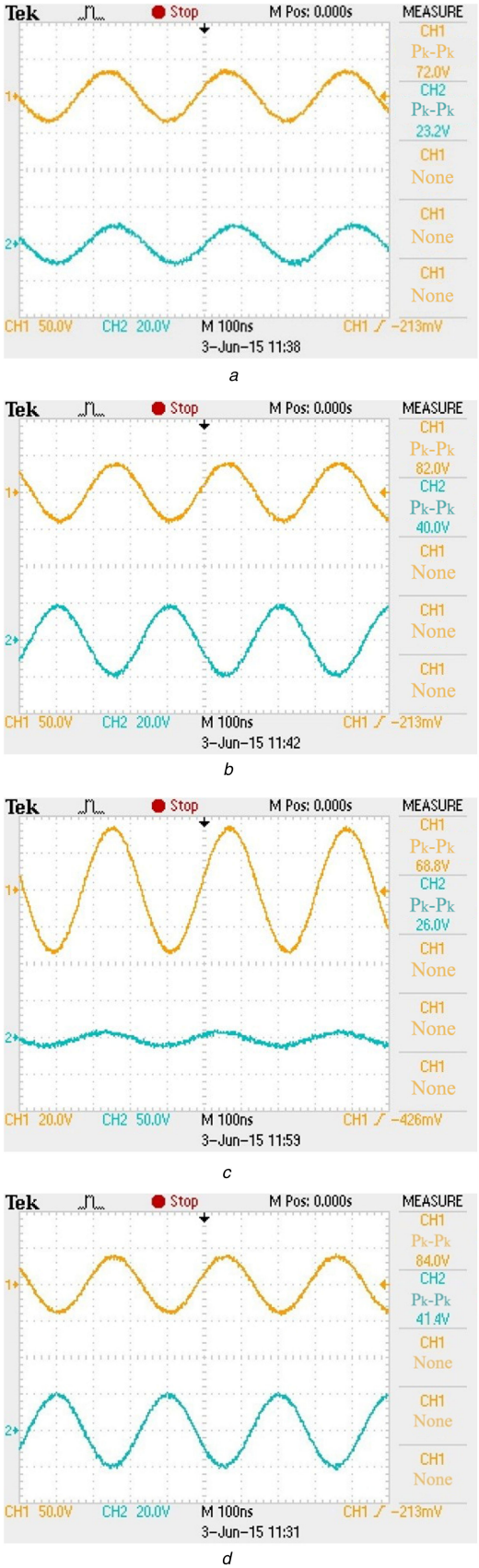

Fig. 5 *Comparison of voltage waveforms*

(a) Voltage waveforms without AFT at central resonance frequency f_0, ***(b)*** Voltage waveforms with AFT at deflected resonance frequency f_1, ***(c)*** Voltage waveforms without AFT at deflected resonance frequency f_1, ***(d)*** Voltage waveforms with AFT at central resonance frequency f_0

Fig. 5*a*, which works at a central resonance frequency f_0. The upper curve represents the voltage waveform of the receiver (peak-to-peak: 82 V), and the lower curve represents the voltage waveform of the receiver (peak-to-peak: 40 V) in Fig. 5*b*, which works at a deflected resonance frequency f_1.

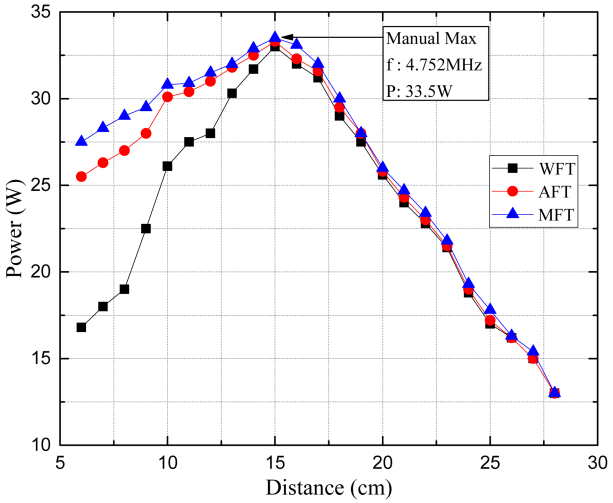

Fig. 6 *Experimental results*

A comparison of Fig. 5*a* with Fig. 5*b*, shows that the AFT system changes the operation frequency of DDS from f_0 to f_1 when the distance changes from 15 to 10 cm, which improves the power of the receiver coil.

The upper curve represents the voltage waveform of the transmitter (peak-to-peak: 68 V) and the lower curve represents the voltage waveform of the receiver (peak-to-peak: 26 V) in Fig. 5*c*, which works at a deflected resonance frequency f_1. The upper curve represents the voltage waveform of the transmitter (peak-to-peak: 84 V), and the lower curve represents the voltage waveform of the receiver (peak-to-peak: 41.4 V) in Fig. 5*d*, which works at a central resonance frequency f_0.

A comparison of Fig. 5*c* with Fig. 5*d*, shows that the AFT system changes the operation frequency of DDS from f_1 to f_0 when the distance changes from 10 to 15 cm, which also improves the power of the receiver coil.

In conclusion, a higher transfer power can be achieved by making a real-time adjustment to the operation frequency when the system works at varying distances. Therefore, real-time frequency tracking is effective in avoiding a decrease in the transfer power.

To illustrate the advantages of IACA, three sets of experiments were conducted. Without frequency tracking (WFT), the power values are captured at a frequency of 4.525 MHz in increments of 1 cm from 6 to 28 cm. With AFT, the corresponding power values are captured in increments of 1 cm from 6 to 28 cm. in addition, the corresponding manual frequency tracking (MFT) results are obtained by adjusting the frequency under the same condition. The experimental results are shown in Fig. 6. The upper line shows the result for manual-control frequency tracking, the middle line shows the result for adaptive frequency control, and the lower line shows the result without frequency tracking. The results show that the result for AFT is obviously better than the result without frequency tracking, and the former can basically achieve the effect of manual-control frequency tracking.

Statistical results for MFT and AFT are listed in Table 2 (see the Appendix for the table of results). The mean value for the manual-control data and frequency-control data are 26.5817 and 26.2004, respectively. The mean deviation is 1.45%. By calculating the error of the manual-control data and frequency-control data, the maximum error is found to be less than 5.00%.

The test results of the variance homogeneity with AFT based on IACA are listed in Table 3 (see the Appendix for the table of results). The F value is 0.008, and the significance probability is 0.931, indicating that there is no significant difference between the variances of AFT and MFT. The double-tailed significant test is 0.843, which is greater than 0.05, indicating that there is no significant difference between the means of MFT and AFT under the 95% confidence interval for the mean difference. In summary,

the above data analysis shows that the AFT based on IACA can alleviate the attenuation of power against distance variations in the case of over coupling, which is the same as MFT.

5 Conclusion

In this paper, an IACA has been proposed, and the pheromones of the path are adaptively adjusted to avoid the local optimum. Simulation results based on MATLAB verified the feasibility of the proposed algorithm. The IACA has good robustness, and can be used in an AFTC system, which varies its operating frequency to enable real-time tracking of a maximum power point. The experimental analysis of three tracking approaches verifies that AFT based on IACA can achieve the results that are similar to MFT. Therefore, frequency-tracking control based on IACA can improve transfer power in the case of over coupling.

6 Acknowledgments

This work was supported by the National Natural Science Foundation of China under grants nos. 51577133, 51477117, 51607121, 51677132, and 51407058. The work is also supported by the Tianjin Research Program of Application Foundation and Advanced Technology (15JCYBJC46700) and the Tianjin Support Program of Science and Technology (15ZCZDGX00980).

7 References

[1] Qingxin, Y., Haiyan, C., Guizhi, X., *et al.*: 'Research progress in contactless power transfer technology', *Trans. China Electrotech. Soc.*, 2010, **25**, (7), pp. 6–13

[2] Wenzhen, F., Bo, Z., Dongyuan, Q., *et al.*: 'Maximum efficiency analysis and design of self-resonance coupling coils for wireless power transfer system', *Proc. CSEE*, 2009, **29**, (18), pp. 21–26

[3] Yue, S., Chenyang, X., Xin, D., *et al.*: 'Analysis and optimization of mutual inductance for inductively coupled power transfer system', *Trans. China Electrotech. Soc.*, 2010, **30**, (33), pp. 44–50

[4] Wenzhen, F., Bo, Z., Dongyuan, Q.: 'Study on frequency-tracking wireless power transfer system by resonant coupling'. Power Electronics and Motion Control Conf., Wu Han, China, 2009, pp. 2658–2663

[5] Kim, Y., Ling, H.: 'Investigation of coupled mode behaviour of electrically small meander antennas', *Electron. Lett.*, 2007, **43**, (23), p. 2007

[6] Teck, C.B., Takehiko, I., Masaki, K., *et al.*: 'Basic study of improving efficiency of wireless power transfer via magnetic resonance coupling based on impedance matching'. 2010 IEEE Int. Symp. on Industrial Electronics, Bari, Italy, July 2010, pp. 2011–2016

[7] Trevor, S.B., Nicholas, R., Ken, W.S.: 'Antenna impedance matching for maximum power transfer in wireless sensor networks'. Sensors, 2009 IEEE, Christchurch, New Zealand, October 2009, pp. 916–919

[8] Kim, N.Y., Kim, K.Y., Ryu, Y.-H., *et al.*: 'Automated adaptive frequency tracking system for efficient mid-range wireless power transfer via magnetic resonance coupling'. Proc. of the 42nd European Microwave Conf., Amsterdam, Netherlands, October 2012, pp. 221–224

[9] Heteng, X., Wangqiang, N., Xiangcheng, M., *et al.*: 'Resonant frequency tracking of contactless power transmission system by a DSP software phase locked loop', *Electr. Drive*, 2012, **42**, (6), pp. 59–62

[10] Fen, L., Huizhen, W.: 'Study of series resonant full-bridge converter based on frequency tracking control', *Power Electron.*, 2010, **44**, (3), pp. 63–67

[11] Hao, Z., Gang, Y., Liwei, M., *et al.*: 'A new method of frequency tracking control for ICPT system', *Power Electron.*, 2013, **49**, (9), pp. 77–79

[12] Rosario, P., Siamak, A., Angelo, R., *et al.*: 'Efficiency optimization of an integrated wireless power transfer system by a genetic algorithm'. 2016 IEEE Applied Power Electronics Conf. and Exposition (APEC), Long Beach, CA, March 2016, pp. 3669–3676

[13] Vittorio, M., Alberto, C.: 'The ant system applied to the quadratic assignment problem', *IEEE Trans. Knowl. Data Eng.*, 1999, **11**, (5), pp. 769–778

[14] Mohammed, O.A., Lowther, D.A., Lean, M., *et al.*: 'On the creation of a generalized design optimization environment for electromagnetic device', *IEEE Trans. Magn.*, 2001, **37**, (5), pp. 3562–3565

8 Appendix

See Tables 1–3.

Table 1 Coil parameters and frequencies of transmitter and receiver

Parameter	Transmitter coil	Receiver coil	Primary oscillator	Secondary oscillator
inductance, μH	1.850	1.850	70.00	70.00
capacitance, pF	685.2	685.2	78.50	78.50
resistance, Ω	1.800	2.100	50.00	50.00
turns (coil)	1.000	1.000	10.00	10.00
wire diameter, mm	2.100	2.100	2.100	2.100
diameter, cm	17.05	17.05	17.05	17.05
resonance frequency, MHz	4.525	4.525	4.525	4.525

Table 2 Statistical description of results

Header	Sample capacity	Mean value	Standard deviation	Stand error of mean
manual frequency tracking	23	26.5817	6.5157	1.3586
adaptive frequency tracking	23	26.2004	6.4639	1.3478

Table 3 Test results of variance homogeneity with AFT

Hypothesis testing	*F*-value	Significance	*T*-value	Double-tail significant	Mean difference	Standard error values
set-equal variance	0.008	0.931	0.199	0.843	0.3813	1.91375